RESEARCH ARTICLE

Fabrication and photocatalytic degradation of reactive blue 19 by $CuWO_4$, Ag_3PO_4, and $CuWO_4$-$Ag3_pO_4$ composites under visible light irradiation

Aliakbar Arabameri, Mohammad Javad Asadollahzadeh*, Hamed Rashidi, Javad Seyfi

Department of Chemical Engineering, Shahrood Branch, Islamic Azad University, Shahrood, Irana

ARTICLE INFO

Article History:
Received 2021-08-07
Accepted 2021-10-15
Published 2021-11-01

Keywords:
Photocatalyst, Reactive Blue 19
Anthraquinone reactive dye,
$CuWO_4$-Ag_3PO_4 Nanocomposite

ABSTRACT

$CuWO_4$ nano-powder was synthesized via a hydrothermal reaction using $CuCl_2.2H_2O$ and $Na_2WO_4.2H_2O$ in the stoichiometric 1:1 Cu:W molar ratio and sodium citrate as raw materials. Also, Ag_3PO_4 was synthesized by a precipitation method using Na_2HPO_4 and $AgNO_3$. Finally, $CuWO_4$-Ag_3PO_4 nanocomposite was synthesized in a precipitation route using the as-synthesized $CuWO_4$ and Ag_3PO_4 as raw materials. The synthesized materials were characterized by the powder X-ray diffraction (PXRD) technique. In order to investigate the effect of concentration of the Basic solutions on the obtained materials,morphology, the synthesized materials' morphologies were studied by field emission scanning electron microscopy (FESEM) technique. As shown by the FESEM images, the $CuWO_4$ material morphology was spherical particles. Besides, the photocatalytic performance of the as-synthesized nanocomposites was studied for the degradation of Reactive Blue 19 (RB19) under direct visible light irradiation. For this purpose, several reaction parameters that affect the degradation yield, such as catalyst amount, pH value, and absence/presence of light, were investigated. The results indicate the higher photocatalytic yield at the presence of light irradiation when the solution's pH value was in the acidic range and the weight percent of silver phosphate in the composite mixture and the catalyst amount was more. The information revealed that a 0.05 g nanocomposite containing 0.24 mmole of Ag_3PO_4, with an initial pH of 3 and 100 mL of RB 19 with 30 mg/L concentration, approximately after 30 min, could remove completely under visible light illumination.

How to cite this article
*Arabameri A., Asadollahzadeh M.J., Rashidi H., Seyfi J. Fabrication and photocatalytic degradation of reactive blue 19 by CuWO4, Ag3PO4, and CuWO4-Ag3PO4 composites under visible light irradiation. J. Nanoanalysis., 2021; 8(4): -10. DOI: 10.22034/jna.***.*

INTRODUCTION

Heterogeneous semiconductor photocatalysis has been actively studied for environmental remediation. Copper tungstate ($CuWO_4$) is belonging to the structurally divalent transition metal tungstates family. This compound contains 3d orbital corresponding to the transition metal [1]. Copper tungstate is a well-known n-type semiconductor with a wide range of applications as scintillation detectors, photoanodes, laser host, electrode material for photoelectrolysis, optical fibers, solar-assisted water splitting, and other usage. Copper tungstate can absorb light at wavelengths up to 540 nm, so it has a narrow bandgap (Eg) of 2.3–2.4 eV. The electronic properties related to $CuWO_4$ crystals have been reported in different fields [2-4]. At room temperature and low pressure, the $CuWO_4$ crystal is an important member of transition metal tungstates, which exhibits a triclinic structure [5].

$CuWO_4$ composites have been widely used for applications such as electrical contacts, arc-resistant electrodes, microwave packages, heavy-duty electrical contacts, microelectronics devices, electro-discharge machining, and heat sinks

* Corresponding Author Email: *m.asadalahzadeh@gmail.com*

This work is licensed under the Creative Commons Attribution 4.0 International License.
To view a copy of this license, visit http://creativecommons.org/licenses/by/4.0/.

materials for high-density integrated circuits. Due to their enhanced mechanical and physical properties, good arc erosion resistance, remarkable thermal and electrical conductivity, and high microwave absorption ability, they can serve in various applications [6,7].

Recently, Ag_3PO_4 has attracted considerable attention as a potentially visible light photocatalyst with a bandgap of 2.45 eV. So, the role of Ag_3PO_4 is a sensitizer absorbing visible light [8]. Silver phosphate (Ag_3PO_4) crystallizes in a body-centered cubic structure (bcc) with space group P-43n. This material has received considerable attention because of its photooxidative applications [9]. Ag_3PO_4 exhibits extremely high photooxidative capabilities for O_2 evolution from water splitting and organic dye decomposition under visible light irradiation. Ag_3PO_4 has a direct bandgap of about 2.43 eV that can absorb energies with wavelengths shorter than about 530 nm. They can achieve a quantum efficiency of about 90% at the near 420 nm wavelengths in water oxidation with $AgNO_3$ as a scavenger [10]. Ag_3PO_4 is the only compound that incorporates nonmetallic p-block specie into Ag_2O [11]. In recent years, silver phosphate (Ag_3PO_4) is a new type of photocatalyst that is highly effective in visible light [12].

One approach to enhance the photocatalytic activity and promote the charge separation efficiency of Ag_3PO_4 is the coupling it with other semiconductors or noble metals. Some coupled systems such as Ag_3PO_4/TiO_2, Ag_3PO_4/AgX (X=Cl, Br, I), Ag_3PO_4/SnO_2, Fe_3O_4/Ag_3PO_4, Ag_3PO_4/Ag, Ag_3PO_4/BiOCl, Ag_3PO_4/reduced graphite oxide sheets, and carbon quantum dots/Ag_3PO_4 composites have recently been developed to improve the photocatalytic activity of Ag_3PO_4 [13]. Besides, some other composite materials of $CuWO_4$ and Ag_3PO_4 nanomaterials, including Ag_3PO_4–ZnO [9], Ag_3PO_4-GO [14], ZnO/$CuWO_4$ [15], CdS-$CuWO_4$-TiO_2 [16], Fe_3O_4/ZnO-$CuWO_4$ [17], Ag_3PO_4/$ZnFe_2O_4$ [18] was reported.

Several methods have been reported for the synthesis of $CuWO_4$ nanomaterials, including hydrothermal method using Na_2WO_4 and $Cu(NO_3)_2.3H_2O$ at 170 °C for 20 h followed by annealing at 500 °C for 3 h [1], precipitation method [2], ultrasonic method [3,4], chemical precipitation method [5], hydrolysis method [6], hydrothermal method for synthesizing $CuWO_4$ film at 180 °C for 8 h followed by annealing at 500 °C for 2 h using $H_2N_{10}O_{41}W_{12}.xH_2O$ and $CuCl_2{\cdot}2H_2O$ [19], microwave method assisted solid state method [20], hydrothermal method at 100 °C for 10 h followed by annealing at 500 °C for 2 h using $Cu(NO_3)_2$ and Na_2WO_4 [21], co-precipitation method [7], hydrothermal method at 110 °C for 2 h followed by annealing at 500 °C using $Cu(O_2CCH_3)_2.H_2O$ and $Na_2WO_4.2H_2O$ as raw materials [15], chemical impregnation method [16], refluxing method [17], hydrothermal method at 180 °C for 18 h followed by annealing at 500 °C using $CuCl_2$ and Na_2WO_4 as raw materials [22], thermochemical method [23], co-precipitation method [24], hydrothermal method at 180 °C for 28 h followed by annealing at 400 - 700 °C for 2h using $Cu(NO_3)_2{\cdot}3H_2O$ and $Na_2WO_4{\cdot}2H_2O$ as raw materials [25], electrochemical method [26, 27]. Besides, several methods have been reported for the synthesis of Ag_3PO_4 materials, including precipitation method using sodium stearate, $AgNO_3$ and $Na_2HPO_4.12H_2O$ agitated for 1h [18], co-precipitation method using $AgNO_3$ and $Na_2HPO_4{\cdot}12H_2O$ agitated for 1h [8], precipitation method $AgNO_3$ and $Na_2HPO_4.12H_2O$ agitated for 1h [9], precipitation method using $AgNO_3$ and $Na_2HPO_4{\cdot}12H_2O$ [10], precipitation method using NaH_2PO_4, Na_2HPO_4, Na_3PO_4 and $AgNO_3$ [12], precipitation method using oleic acid, $AgNO_3$ and H_3PO_4 [13], precipitation method using $AgNO_3$ and Na_2HPO_4 [14], precipitation method using Ag_2CO_3 and Na_2HPO_4 [28], precipitation method using oleic acid, and $AgNO_3$, Na_2HPO_4 [29].

Anthraquinone-based dyes are more resistant to biodegradation because of their fused aromatic structures compared to azo-based ones [30]. Also, they may cause acute toxicity or even mutagenic effects on aquatic organisms [31]. Therefore, anthraquinone reactive dyes have gradually attracted significant attention from the toxicological and environmental perspectives, particularly considering the current increase in their applications.

Reactive Blue 19 (RB-19) is a commercially representative anthraquinone reactive dye. Few past studies concerning ozonation of RB-19 solution were focused on decolorization efficiency and color removal kinetics [32]. Our previous work has investigated the transformation of RB-19 under different ozonation conditions in 10 min of reaction time and found that partial oxidation was obtained [33]. Several catalysts have been reported for the photodegradation of RB 19, including $K_2S_2O_8$ [34], TiO_2 [35], ozonation [36], and bacterial flora [37].

In the present work, the synthesis of CuWO4 via hydrothermal method at 180 °C for 18h followed

by calcination at 500 °C for 2h using $CuCl_2.2H_2O$ and $Na_2WO_4.2H_2O$ in the stoichiometric 1:1 Cu:W molar ratio as raw materials is reported. Besides, Ag_3PO_4 is prepared by a simple precipitation method at 80 °C for 1 h using Na_2HPO_4 and $AgNO_3$ as raw materials. Also, several $CuWO_4$-Ag_3PO_4 composites with different molar ratios are prepared in the present work. The obtained materials are characterized by the PXRD technique. Besides, the morphology of the obtained materials is studied by FESEM images. Also, the photocatalytic degradation of RB 19 was investigated under direct visible light irradiation without using H_2O_2 (Scheme 1). Failure to utilize oxidants such as ozone (O_3) and Hydrogen peroxides (H_2O_2) in the photocatalytic degradation process will reduce the risks of using these materials due to high corrosion, reduce costs due to high prices of these materials and respect for all living things on the earth. Reducing the cost of initial preparation of the effluent to remove the paint and eliminating the cost of neutralizing it are another advantages. Effects of reaction parameters such as pH value of the dye solution and catalyst amount on the photocatalytic efficiency are also studied.

EXPERIMENTAL

Materials and methods

All chemicals were of analytical grade, obtained from commercial sources, and used without further purification. Phase identifications were performed on a powder X-ray diffractometer D5000 (Siemens AG, Munich, Germany) using CuK_α radiation. The morphology of the obtained materials was examined with a Philips XL30 scanning electron microscope (Philips, Amsterdam, Netherlands). Absorption spectra were recorded on an Analytik Jena Specord 40 (Analytik Jena AG Analytical Instrumentation, Jena, Germany). The concentration of reactive blue 19 was determined at 600 nm using a Shimadzu UV-visible1650 PC spectrophotometer. A BEL PHS-3BW pH-meter with a combined glass-Ag/AgCl electrode was used to adjust the solution pH.

Synthesis of $CuWO_4$ nanomaterial

In a typical experiment, 2.045 g (0.02 mol) of $CuCl_2.2H_2O$ was added into 25 mL deionized water in a 100 mL beaker under stirring until the salt was solvated. When the salt was dissolved, sodium citrate (0.29 g or 1.0 mmol) was added to the resultant solution under stirring. The obtained mixture was stirred continuously for 30 min. Then 10 mL deionized water was added to the obtained solution. $Na_2WO_4.2H_2O$ (6.788 g or 0.02 mol) was added to the solution, and 5 mL of deionized water was combined with the mixture. The mixture was stirred for 30 min and was transferred to a Teflon-lined autoclave. Then the autoclave was sealed and treated thermally at 180 °C for 18 h. After the desired reaction time, the autoclave was cooled generally to room temperature. Then the precipitate was filtered and washed with deionized water and ethanol, respectively. The final powder was dried at 90 °C for 3h. Finally, produced dried powder was

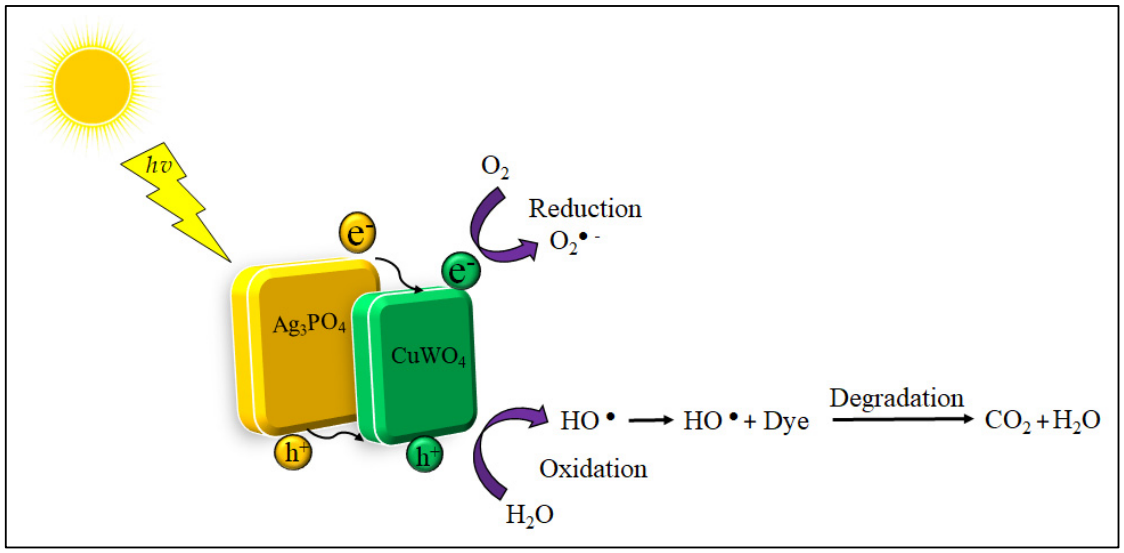

Scheme 1. Photocatalytic degradation of RB 19.

(cc) BY

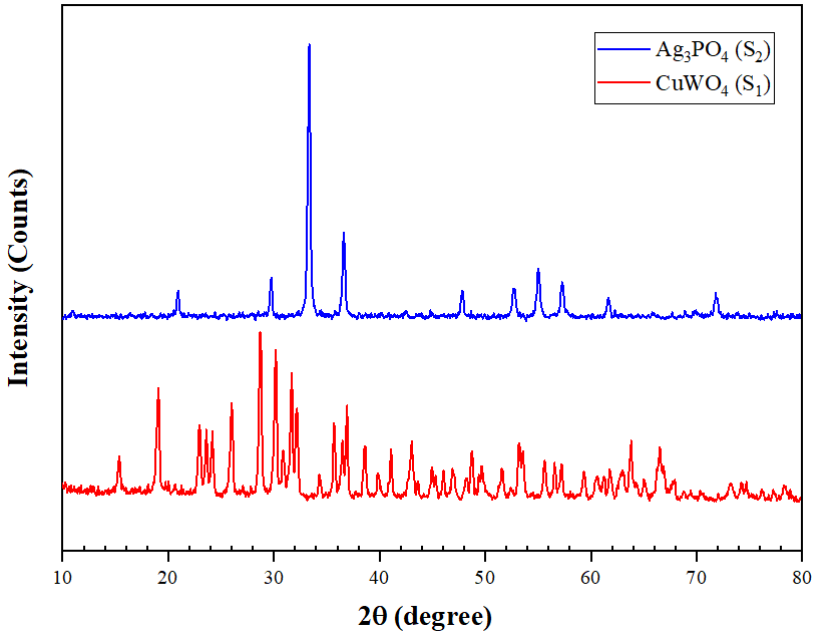

Fig. 1. PXRD patterns of a) S_1 and b) S_2.

annealed at 500 °C for 2h. The synthesis yield was 86% for CuWO4 nanomaterial (S_1).

Synthesis of Ag_3PO_4 nanomaterial

Na_2HPO_4 (0.3549 g or 2.5 mmol) and $AgNO_3$ (0.84935g or 5 mmol) were dissolved in 50 mL of deionized water, separately in two beakers. The obtained solution was stirred for 10 min. Then Na_2HPO_4 solution was transferred into a burette. The $AgNO_3$ was titrated with the Na_2HPO_4 solution (25 drops per min). The titrated solution was then heated at 80 °C for 1h. The obtained precipitate was filtered and washed with deionized water. The final powder was dried at 100 °C for 1h. The synthesis yield was 75% for Ag_3PO_4 nanomaterial (S_2).

Synthesis of $CuWO_4$-Ag_3PO_4 nanocomposites

A certain amount of $CuWO_4$ (0.97 g or 3.10 mmol) (S_3), (0.95 g or 3.05 mmol) (S_4), and (0.9 g or 2.89 mmol) (S_5) were added in an 80 mL of deionized water existent in the beaker and was stirred for 90 min. In another beaker containing 5 mL deionized water, a specific amount of Ag_3PO_4 (0.03 g or 0.07 mmol), (0.05 g or 0.12 mmol), and (0.1 g or 0.24 mmol) was added and stirred for 30 min. Afterward, the two beakers were mixed in each other, and the obtained solution was heated until it was boiled. Then the solution was refluxed for 90 min. The produced precipitate was filtered and washed three times with deionized water. The obtained powder was dried at 90 °C for 3 h.

RESULTS AND DISCUSSION

Characterization

The X-ray diffraction patterns of the $CuWO_4$ (S_1) (JCPDS No 88-0269) and Ag_3PO_4 (S_2) (JCPDS No. 06-0505) are reported in Fig. 1. According to the structural analysis of Ag_3PO_4 nanoparticles using x-ray diffraction, five strong peaks at 33.38 °, 36.74 °, 52.73 °, 55.064 °, and 57.3080 ° are observed, which are in accordance with the standard (JCPDS No. 06-0505) and Indicates the formation of Ag_3PO_4 structure. Similarly, for $CuWO_4$ nanoparticles, five strong peaks of 27.72 °, 30.11 °, 31.58 °, 48.65 °, and 53.1940 ° are observed, which are in accordance with the standard (JCPDS No. 88-0269) and indicate the formation of $CuWO_4$. In addition, the XRD patterns of the prepared composites (S_3, S_4, and S_5) are reported in Fig. 2. The results show that the patterns for S_1 and S_2 have a main $CuWO_4$ crystal structure with space group P-1. Lattice parameters were found as a = 4.87 Å, b = 5.82 Å and c = 4.68 Å with $\alpha = 88.35, \beta = 92.50$ with $\gamma = 97.20$ ° [1-5]. Besides, the PXRD pattern of S_3 shows that Ag_3PO_4 crystallizes in the cubic crystal system with space group P-43n. The lattice parameters were found as a = b = c = 5.99 Å [8-13].

Fig. 2 shows the PXRD patterns of S_3 to S_5. It

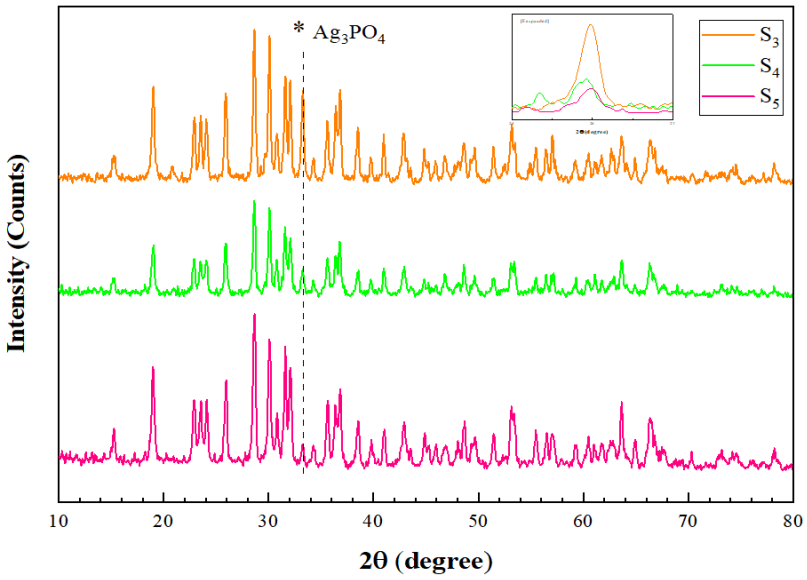

Fig. 2. PXRD patterns of a) S_3, b) S_4, and c) S_5.

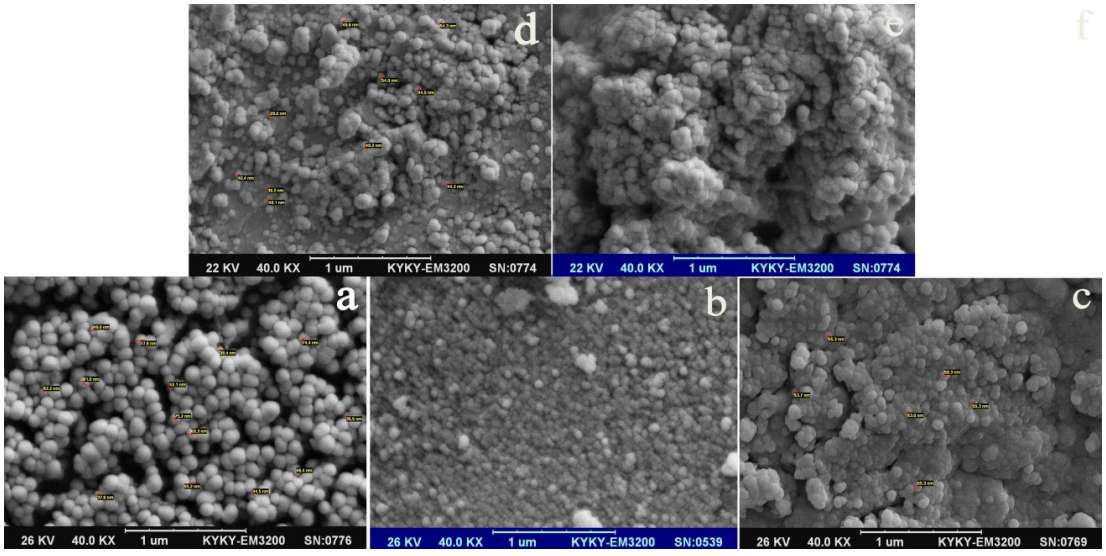

Fig. 3. FESEM images of a) S_1, b) S_2, c) S_3, d) S_4, and e) S_5.

was found that the crystal phase growth decreased with increasing the Ag_3PO_4 ratio to $CuWO_4$ in the composite material, and Fig. 2 confirms the conclusion. Besides, it shows that when the weight percent of Ag_3PO_4 was increased from 3% (S_3) to 5% (S_4), the peak shifts toward the lower 2θ value. It shows an expansion in the crystal system, but when increasing the Ag_3PO_4 value to 10% (S_5), the peak shifts toward the higher 2θ value. So there is a contraction in the unit cell.

Fig. 3 shows the FESEM images of S_1–S_5 nanomaterials. The image of $CuWO_4$ nanomaterial showed that the morphology of the obtained material was a spherical particle with a highly homogeneous morphology (a). The FESEM image of the synthesized Ag_3PO_4 nanomaterial showed that the morphology of the target was particles with homogeneous morphology (b). Fig. 3d-f shows the

(cc) BY

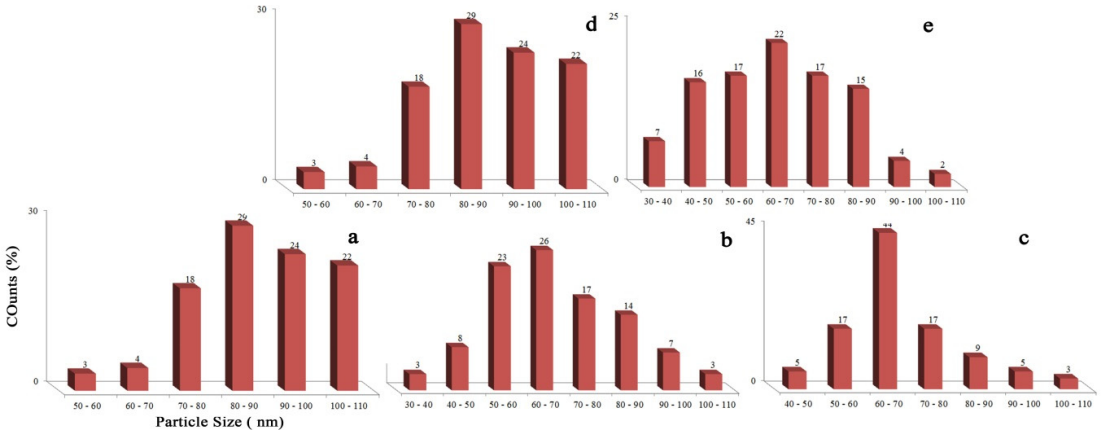

Fig. 4. Particle size distribution profiles of a) S_1, b) S_2, c) S_3, d) S_4 and e) S_5.

FESEM images of S_3 – S_5. The images show that the targets' morphology was changed with increasing the weight percent of Ag_3PO_4 in the composite mixture. It was found that the morphology of the target was highly homogeneous spherical particles when the weight percents were 3 and 5 %. However, the morphology of the target was changed to particles in which the targets' morphology was heterogeneous.

Fig. 4a – f shows the particle size distribution profiles of S_1–S_5, respectively. The data for the size distribution of $CuWO_4$ showed that the maximum particle diameter is 80–90 nm. For Ag_3PO_4, it can be seen the high homogeneity of the particle size, and the maximum size range was 60–70 nm. Fig. 4c – e shows the data for the composite nanomaterials. The data indicate that the maximum diameter sizes were about 80–90, 60–70, and 60–70 nm for S_3, S_4, and S_5, respectively. The average particle sizes were decreased with increasing Ag_3PO_4 weight percent in the composite material.

we calculated the mean size of crystalline domains with the Scherrer equation ($\tau = \frac{K\lambda}{\beta \cos\theta}$) and compared with this parameter from FE-SEM. The results show that the mean-size particles of larger crystals form nanometer-sized particles with larger sizes and the results are consistent with each other. According to XRD patterns data belong to $CuWO_4$ and Ag_3PO_4, maximum FWHM occurs in 2θ=96.72, and 0.72 intensity and 2θ=65.72 and 0.7085 results are related to the average size of its crystals have been achieved 17.33 nm and 13.89 respectively. Mean-size by FE-SEM for $CuWO_4$ and Ag_3PO_4 nanomaterials 80-90 nm and 60-70 nm have been identified, respectively.

Photocatalytic activity

The synthesized samples' photocatalytic activity was investigated for the degradation of RB 19 (Anthraquinone dye) under direct visible light irradiation. A light filter was used to prevent wavelengths below 400 nm. In order to prepare a 30 ppm RB 19 dye solution, 0.03 g of RB 19 powder was dissolved in 1000 mL of deionized water. The pH value of the dye solution was adjusted to the desired amount using 1M of HCl or NaOH solutions. In a typical photocatalytic process under the visible light irradiation, a certain amount (g) of the synthesized sample was added into 100 mL of the as-prepared solution and sonicated for 10 min in a dark room to establish an adsorption/desorption equilibrium between RB 19 molecules and the surface of the photocatalyst followed by further magnetic stirring (250 rpm) under direct visible light irradiation. The solution was drawn out at a certain time, and the photocatalyst was separated by centrifugation to measure the absorption spectra of RB 19 and calculate the RB 19 concentration using UV-Vis spectrophotometry. The following formula calculated the photodegradation yield (%) of RB 19:

$$\left(\frac{A_0\text{-}A_t}{A_0}\right) \times 100$$

That in this equation, A_0 and A_t represents the initial absorbance of RB 19 at 602 nm and the absorbance at time t, respectively.

In order to study the degradation of RB 19 in a dark room under the typical catalytic degradation process, some tests were done. Figs. 5a and 5b

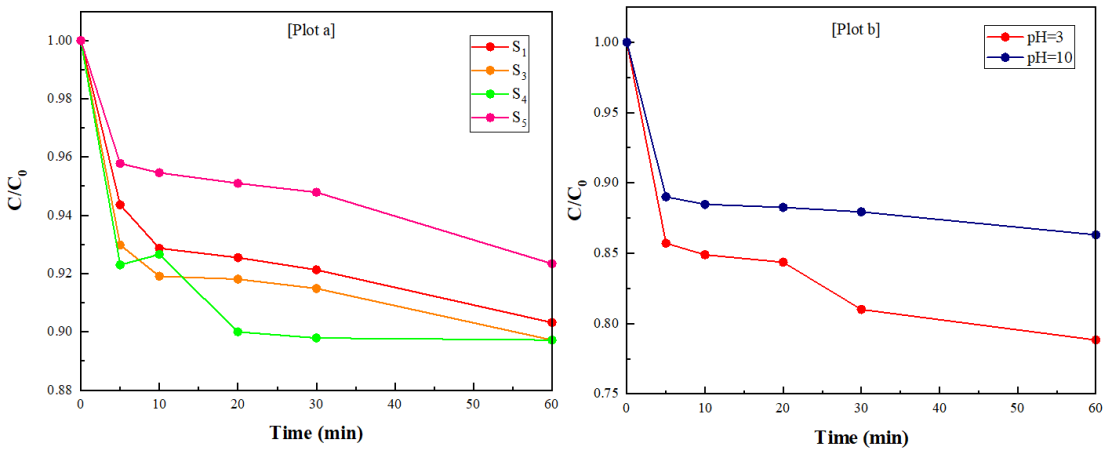

Fig. 5. Plots of the photodegradation of RB 19 at the dark-room (a) the degradation efficiency for different nanocomposites (Reaction condition: pH= 6, 100 mL of 30 ppm dye solution and 0.05 g of catalyst) and (b) the effect of solution pH value on the degradation yield for the reference composite s_5 (Reaction condition: 100 mL of 30 ppm dye solution and 0.05 g of catalyst).

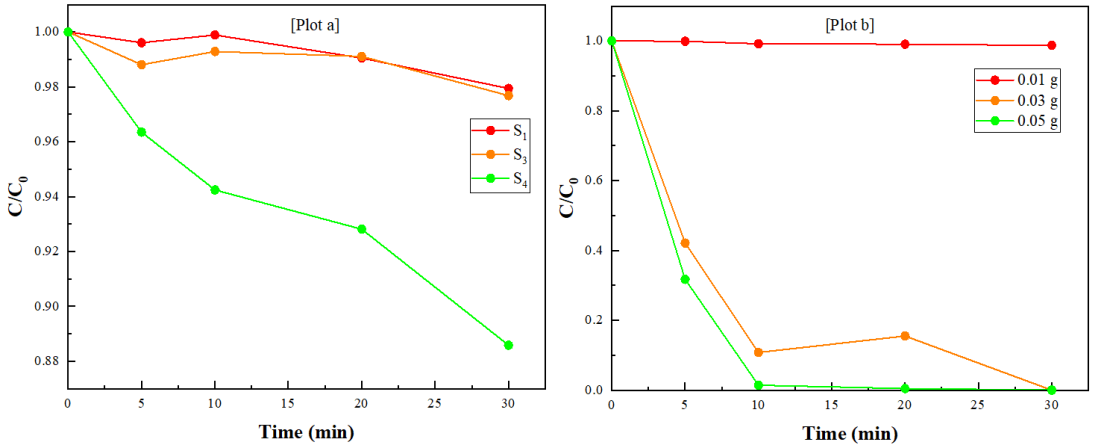

Fig. 6. Plots of the photodegradation of RB 19 under direct visible light irradiation(a)degradation yield for the synthesized nanocomposites (Reaction condition: 0.03 g of catalyst, pH=6, 100 mL of 30 ppm dye solution) and b) effect of catalyst amount on the degradation yield for the reference composite s_5 (Reaction condition: pH=3, 100 mL of 30 ppm dye solution).

indicate the degradation of RB 19 using the various synthesized samples in different pH values and under dark conditions, respectively. The data in Fig. 5a indicates that there was no considerable degradation in the dark-room. Also, Fig. 5b reveals that by changing the pH value from acidic to basic condition, the degradation of RB 19 decreased. However, the degradation percent was still lower than under the dark condition. So, it can be concluded the degradation yield under dark-room for the samples in any solution pH was not considerable.

The results in photocatalytic degradation of RB 19 under direct visible light irradiation shows that the degradation yield of the as-prepared nanomaterials was increased by increasing Ag_3PO_4 weight percent in the nanocomposite mixture (Fig. 6a). It is found that under direct visible light irradiation when the catalyst weight in the reaction mixture is increased, the considerably higher degradation yield of RB 19 can be achieved. It can be concluded that the surface area that exists for the adsorb dye onto the catalyst surface is increased, and so the degradation in a certain time is done faster. However, it is clear that 0.03 g of catalyst in the reaction mixture can be the optimum value.

Fig. 7a and 7b presents the effect of the solution pH value on the degradation yield under the visible

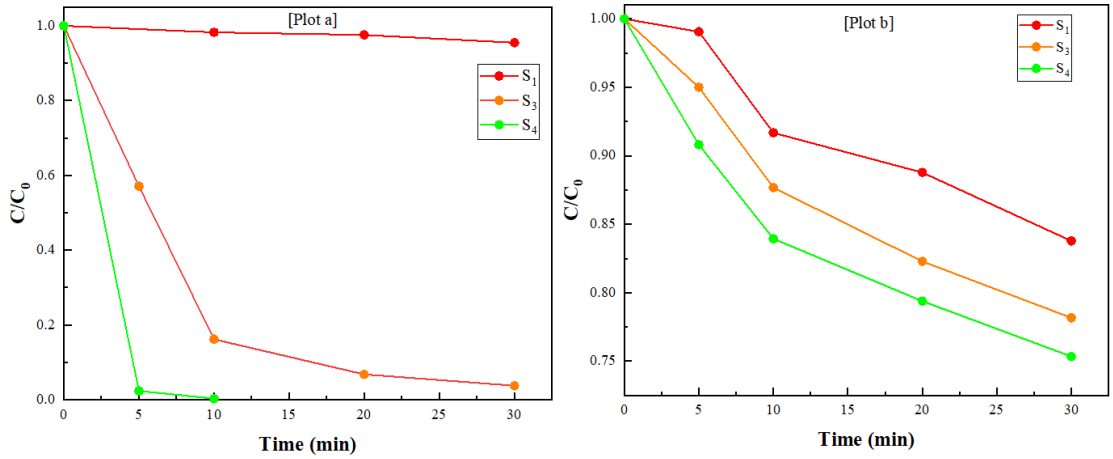

Fig. 7. The efficiency of degradation yield of the as-synthesized nanomaterials when (a) the pH value is 3 and (b) the pH value is 10 (Reaction condition: 0.03 g of catalyst, 100 mL of 30 ppm dye solution).

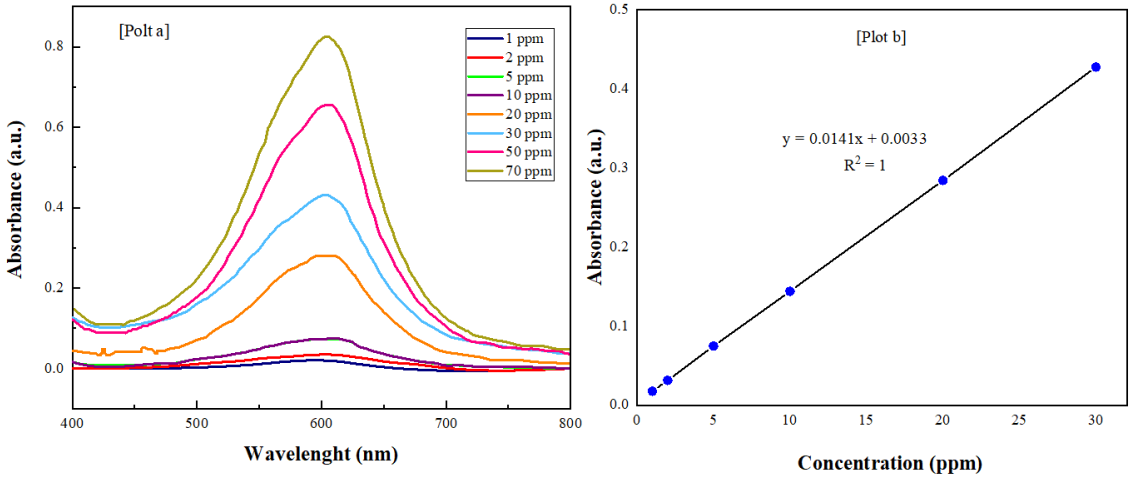

Fig. 8. Plots of a) UV-Vis spectra of RB 19 solutions and b) calibration curve of the as-prepared solutions.

light irradiation. Fig. 7a indicates that when the pH value was in the acidic range, the degradation yield increased for the samples in which the weight percent of Ag_3PO_4 was more. The observation indicates that existing H^+ in the solution activated the oxidizing agents, so the degradation was done faster. Fig. 7b shows that when the solution pH value was in the basic range, the degradation yield of all of the samples decreased considerably. Besides, we had mentioned in Fig. 6a that when the pH value of the solution was in the neutral range, the degradation yield is low. The acidic medium increases the performance of the photo-degradation reaction because of change in the surface charges of the nanoparticles. Indeed, this surface charge leads to better dispersion of the nanoparticles in the suspension. As a result, the reaction between the dissolved oxygen and the organic compound will improve and the rate of free radical generation boosts accordingly. However, it is clear that the yield is more of the sample in which the weight percent of Ag_3PO_4 is more (S_4). So, we can conclude that the pH=3 is the optimum value.

Fig. 8a and 8b presents the UV-Vis spectra and calibration diagram of the as-prepared RB 19 dye solution. The data reveal that there is no sensitive error in the preparation process of the dye solutions.

CONCLUSION

This study described the hydrothermal and

precipitation syntheses of highly crystalline $CuWO_4$, Ag_3PO_4, and $CuWO_4$-Ag_3PO_4 nanomaterials. Considering the importance of removing rhodamine B dye from effluents and the problems caused by their presence in water sources, it is necessary to create methods to remove this dye type. The PXRD patterns indicated that the targets were crystallized well in triclinic ($CuWO_4$) and cubic (Ag_3PO_4) crystal systems. The patterns showed that the unit cells were expanded by increasing the Ag_3PO_4 weight ratio in the composite mixture. The particle size distribution data showed that the diameter size ranges were decreased considerably by increasing the Ag_3PO_4 weight percent in the synthesized nanocomposite. FESEM images showed that Ag_3PO_4 weight percent for the synthesis of composite materials has the main effect on synthesizing $CuWO_4$-Ag_3PO_4 nanocomposites. The RB 19 photocatalytic degradation data revealed that a 0.05 g nanocomposite containing 0.24 mmole of Ag_3PO_4, with an initial pH of 3 and Rhodamine B volume and concentration of 100 mL and 30 mg/L, respectively, could achieve removal of 100 % after 30 min under visible light illumination without using H_2O_2. One of the advantages of this work is performing a photocatalytic process without H_2O_2, which reduces the cost of initial preparation of the effluent to remove the dye and, after removal, does not include the cost of neutralizing it and this work could lead to further extensive research on the subject.

CONFLICT OF INTEREST

The authors declare that there is no conflict of interest regarding the publication of this manuscript.

REFERENCE

[1] Chen, H., W. Leng, and Y. Xu, *Enhanced visible-light photoactivity of $CuWO_4$ through a surface-deposited CuO.* The Journal of Physical Chemistry C, **2014**. 118(19): p. 9982-9989.

[2] Xiong, X., H. Chen, and Y. Xu, *Improved photocatalytic activity of TiO_2 on the addition of $CuWO_4$.* The Journal of Physical Chemistry C, **2015**. 119(11): p. 5946-5953.

[3] Dutta, D.P., et al., *Selective sorption and subsequent photocatalytic degradation of cationic dyes by sonochemically synthesized nano CuWO4 and $Cu_3Mo_2O_9$.* RSC advances, **2015**. 5(115): p. 94866-94878.

[4] Pourmortazavi, S.M., et al., *Facile chemical synthesis and characterization of copper tungstate nanoparticles.* Journal of Inorganic and Organometallic Polymers and Materials, **2014**. 24(2): p. 333-339.

[5] Hosseinpour-Mashkani, S.M. and A. Sobhani-Nasab, *Simple synthesis and characterization of copper tungstate nanoparticles: investigation of surfactant effect and its photocatalyst application.* Journal of Materials Science: Materials in Electronics, **2016**. 27(7): p. 7548-7553.

[6] Chen, H., et al., *Improved visible light photocatalytic activity of WO_3 through $CuWO_4$ for phenol degradation.* Applied Surface Science, **2016**. 389: p. 491-495.

[7] Hashempour, M., et al., *Chemical mechanism of precipitate formation and pH effect on the morphology and thermochemical co-precipitation of W–Cu nanocomposite powders.* Materials Chemistry and Physics, **2010**. 123(1): p. 83-90.

[8] Botelho, G., et al., *Experimental and theoretical study on the structure, optical properties, and growth of metallic silver nanostructures in Ag_3PO_4.* The Journal of Physical Chemistry C, **2015**. 119(11): p. 6293-6306.

[9] Dong, C., et al., *Synthesis of Ag_3PO_4–ZnO nanorod composites with high visible-light photocatalytic activity.* Catalysis Communications, **2014**.46 p. 32-35.

[10] Chen, X., Y. Dai, and X. Wang, *Methods and mechanism for improvement of photocatalytic activity and stability of Ag_3PO_4: a review.* Journal of Alloys and Compounds, **2015**. 649: p. 910-932.

[11] CHENG, F., et al., *Research progress of Ag_3PO_4-based photocatalyst: Fundamentals and performance enhancement.* Transactions of Nonferrous Metals Society of China, **2015**. 25(1): p. 112-121.

[12] Amornpitoksuk, P., et al., *Effect of phosphate salts (Na_3PO_4, Na_2HPO_4, and NaH_2PO_4) on Ag_3PO_4 morphology for photocatalytic dye degradation under visible light and toxicity of the degraded dye products.* Industrial & Engineering Chemistry Research, **2013**. 52(49): p. 17369-17375.

[13] Dong, P., et al., *Facile synthesis of tetrahedral Ag_3PO_4 mesocrystals and its enhanced photocatalytic activity.* Materials Research Bulletin, **2014**. 60: p. 682-689.

[14] Chen, X.-j., et al., *Synthesis and characterization of Ag_3PO_4 immobilized with graphene oxide (GO) for enhanced photocatalytic activity and stability over 2,4-dichlorophenol under visible light irradiation.* Journal of hazardous materials, **2015**. 292: p. 9-18.

[15] Mavrič, T., et al., *Design of a highly photocatalytically active ZnO/$CuWO_4$ nanocomposite.* Journal of colloid and interface science, **2016**. 483: p. 93-101.

[16] Vignesh, K., et al., *Fabrication of CdS and $CuWO_4$ modified TiO_2 nanoparticles and its photocatalytic activity under visible light irradiation.* Journal of Industrial and Engineering Chemistry, **2014**. 20(2): p. 435-443.

[17] Shekofteh-Gohari, M. and A. Habibi-Yangjeh, *Fabrication of novel magnetically separable visible-light-driven photocatalysts through photosensitization of Fe_3O_4/ZnO with $CuWO_4$.* Journal of Industrial and Engineering Chemistry, **2016**. 44: p. 174-184.

[18] Chen, X., Y. Dai, and W. Huang, *Novel Ag_3PO_4/$ZnFe_2O_4$ composite photocatalyst with enhanced visible light photocatalytic activity.* Materials Letters, **2015**. 145: p. 125-128.

[19] Tang, Y., et al., *Enhancement of the photoelectrochemical performance of $CuWO_4$ films for water splitting by hydrogen treatment.* Applied Surface Science, **2016**. 361: p. 133-140.

[20] Kumar, R.D. and S. Karuppuchamy, *Microwave-assisted synthesis of copper tungstate nano-powder for supercapacitor applications.* Ceramics International, **2014**. 40(8): p. 12397-12402.

[21] Wei, C., et al., *Soft-template hydrothermal systhesis of*

nanostructured copper(II) tungstate cubes for electrochemical charge storage application. Electrochimica Acta, **2016**. 220: p. 156-163.

[22] Liang, L., et al., *Fabrication of novel $CuWO_4$ hollow microsphere photocatalyst for dye degradation under visible-light irradiation.* Materials Letters, **2016**. 182: p. 302-304.

[23] Hashempour, M., et al., *Thermochemical preparation of W–25% Cu nanocomposite powder through a CVT mechanism.* Materials characterization, **2009**. 60(11): p. 1232-1240.

[24] ReddyPrasad, P. and E.B. Naidoo, *Ultrasonic synthesis of high fluorescent C-dots and modified with $CuWO_4$ nanocomposite for effective photocatalytic activity.* Journal of Molecular Structure, **2015**. 1098: p. 146-152.

[25] Ma, D., et al., *Synthesis and hydrogen reduction of nano-sized copper tungstate powders produced by a hydrothermal method.* International Journal of Refractory Metals and Hard Materials, **2014**. 46: p. 152-158.

[26] Pourmortazavi, S.M., et al., *Taguchi method assisted optimization of electrochemical synthesis and structural characterization of copper tungstate nanoparticles.* International Journal of Refractory Metals and Hard Materials, **2015**. 51: p. 29-34.

[27] Zhang, W., et al., *Cyclic voltammetry analysis of copper electrode performance in Na_2WO_4 solution and optical property of electrochemical synthesized $CuWO_4$ nanoparticles.* Journal of Alloys and Compounds, **2017**. 690: p. 221-227.

[28] Wan, J., et al., *Facile synthesis of porous Ag_3PO_4 nanotubes for enhanced photocatalytic activity under visible light.* Applied Surface Science, **2015**. 355: p. 615-622.

[29] Wang, N., et al., *A g-C3N4 supported graphene oxide/Ag_3PO_4 composite with remarkably enhanced photocatalytic activity under visible light.* Catalysis Communications, **2016**. 73: p. 74-79.

[30] Deng, D., et al., *Decolorization of anthraquinone, triphenylmethane and azo dyes by a new isolated Bacillus cereus strain DC11.* International Biodeterioration & Biodegradation, **2008**. 62(3): p. 263-269.

[31] Novotný, Č., et al., *Comparative use of bacterial, algal and protozoan tests to study toxicity of azo-and anthraquinone dyes.* Chemosphere, **2006**. 63(9): p. 1436-1442.

[32] Hsu, Y.-C., Y.-F. Chen, and J.-H. Chen, *Decolorization of dye RB-19 solution in a continuous ozone process.* Journal of Environmental Science and Health, Part A, **2004**. 39(1): p. 127-144.

[33] Fanchiang, J.M. and D.H. Tseng, *Decolorization and transformation of anthraquinone dye Reactive Blue 19 by ozonation.* Environmental technology, **2009**. 30(2): p. 161-172.

[34] Rezaee, A., et al., *Photochemical oxidation of reactive blue 19 dye (RB19) in textile wastewater by UV/$K_2S_2O_8$ process.* Journal of Environmental Health Science & Engineering, **2008**. 5(2): p. 95-100.

[35] Bakar, F.A., et al., *Investigation of the photodegradation of Reactive Blue 19 on P-25 titanium dioxide: effect of experimental parameters.* Australian Journal of Chemistry, **2015**. 68(3): p. 471-480.

[36] Fanchiang, J.-M. and D.-H. Tseng, *Degradation of anthraquinone dye CI Reactive Blue 19 in aqueous solution by ozonation.* Chemosphere, **2009**. 77(2): p. 214-221.

[37] Xie, X., et al., *Highly efficient biodegradation of reactive blue 19 under the activation of tea residue by a newly screened mixed bacterial flora $DDMY_2$.* RSC advances, **2019**: p. 24791-24801.

CC BY